Arabian Journal of Chemistry (2023) **16**, 104811

King Saud University

Arabian Journal of Chemistry

www.ksu.edu.sa
www.sciencedirect.com

ORIGINAL ARTICLE

An environmentally safe approach for the facile synthesis of anti-mutagenic fluorescent quantum dots: Property investigation and the development of novel antimicrobial applications

Morteza Yazdani [a], **Fereshteh Jookar Kashi** [b,*], **Elahe Seyed Hosseini** [c]

[a] *Department of Phytochemistry, Faculty of Chemistry, University of Kashan, Kashan, Iran*
[b] *Department of Cell and Molecular Biology, Faculty of Chemistry, University of Kashan, Kashan, Iran*
[c] *Gametogenesis Research Center, Kashan University of Medical Science, Kashan, Iran*

Received 15 October 2022; accepted 11 March 2023
Available online 18 March 2023

KEYWORDS

Teucrium polium L.;
Silver quantum dots;
Fluorescent;
Mutagenicity;
Cytotoxicity;
Antimicrobial activity

Abstract Quantum dots as nanocrystals of semiconductor materials are synthesized with different methods. The green synthesis of fluorescent quantum dots using natural stabilizing agents has attracted much attention. This research aims to study the ability of *Teucrium polium* L. extract to green synthesize fluorescent silver quantum dots (AgQDs). The green synthesis of AgQDs was proved using UV–Visible spectrophotometer, Fourier Transform Infrared spectroscopy (FTIR), X-Ray Diffraction (XRD), Transmission Electron Microscopy (TEM), Scanning Electron Microscopy (SEM), Energy-Dispersive X-ray spectroscopy (EDX), Photoluminescence (PL) analysis, and Dynamic Light Scattering (DLS). According to the findings, the shape of fluorescent AgQDs was spherical, and the maximum abundance of particle size distribution was between 3 and 5 nm. Thereupon, antimicrobial, anti-mutagenicity, anticancer, and antioxidant activities were evaluated to distinguish the biological features of AgQDs. Gram-positive bacteria (*S. epidermidis*, MIC: 31.25 μg/ml) and fungi (*C. albicans*, MIC: 31.25 μg/ml) were the most susceptible to AgQDs. Moreover, the AgQDs solution had higher antimicrobial activity than $AgNO_3$. The Ames test demonstrated that AgQDs have considerable anti-mutagenic activities (% mutagenicity inhibition greater than 40) and are not mutagenic. The anticancer activity of AgQDs was distinguished using MTT and brine shrimp lethality (BSL) assays. The analysis indicated that AgQDs had a strong potential for cytotoxicity (BSL: LC_{50} = 2.4 μg/ml, MTT: IC_{50} = 0.8 μg/ml). Further, AgQDs were used for bioimaging human ovarian OVCAR3 cells, and their biocompatibility was

* Corresponding author at: University of Kashan, Qotb-e Ravandi Blvd, Kashan, Isfahan, Iran.
E-mail address: jookar@kashanu.ac.ir (F. Jookar Kashi).

Peer review under responsibility of King Saud University.

Production and hosting by Elsevier

https://doi.org/10.1016/j.arabjc.2023.104811

remarkable. In the DPPH assay, AgQDs displayed high antioxidant activity (89.9% inhibition). Using AgQDs to coat materials to develop antibacterial agents revealed significant activity against *C. albicans* and *S. epidermidis* strains. Our results indicate that *T. polium* is a promising source for synthesizing AgQDs. Due to the potent bioactivities of AgQDs, they can be used in medicine and industry.

1. Introduction

Nanoscience is growing rapidly because of its high potential application in various electronics and cosmetics fields. Nanotechnology is a field of study that deals with nanoparticles (three-dimensional particles having a diameter of 1–100 nm). This could be used in various industries, including dentistry, textiles, catalysis, mirrors, optics, photography, electronics, and food (Shameli et al., 2012). Today, the chemical synthesis methods of nanoparticles are limited due to the use of highly toxic chemicals for living organisms and the environment. However, biological methods are an excellent alternative to chemical methods (Kalimuthu et al., 2020). Some studies have shown that biological methods can overcome this problem. For some years, there have been reports of biological techniques for the synthesis of Ag nanoparticles utilizing organisms such as bacteria (Elbahnasawy et al., 2021), yeast (He et al., 2013), and fungi (Agressott et al., 2020). While microorganisms, including bacteria, fungi, yeasts, and actinomycetes, are still being investigated to produce metallic nanoparticles, utilizing complete plants for nanoparticle biosynthesis is an intriguing sector largely untapped (Vanlalveni et al., 2021). These methods have demonstrated great attention when compared to chemical processes. Metal nanoparticles have been synthesized using phenolic acids as reducing agents, including caffeic acid, ellagic acid, protocatechuic acid, and gallic acid (Ali et al., 2018; Aromal et al., 2012; Edison and Sethuraman, 2012; Mohan Kumar et al., 2012). Consequently, plant extracts as a natural reducing agent are appreciably used in the environmentally friendly synthesis of nanoparticles. Previous studies reported the synthesis of different metallic nanoparticles, including silver nanoparticles, using extracts from seeds, flowers, and roots of various plants. The silver nanoparticles with different sizes and shapes had antimicrobial activity against various microorganisms (Jadoun et al., 2021; Vanlalveni et al., 2021).

This study investigated the water fraction of *T. polium* L. root extract for synthesized AgQDs. This plant belongs to Lamiaceae (Labiatae) family and plant species distributed to Europe and the Mediterranean to West Asia. It is a deciduous shrub growing to 0.2 m. We evaluate some previous work and propose a new natural origin for producing AgQDs because it functions as a reducing and stabilizing agent. Silver quantum dots were characterized and evaluated for their anti-mutagenic, cytotoxic, antimicrobial, and antioxidant activity. Also, we investigated the development of silver coatings on different materials to increase their antimicrobial activity. The most important advantage of this method is that it can perform very well in the green synthesis of AgQDs because it is environmentally friendly, affordable, free of harmful substances, and takes less time. Furthermore, no stabilizer is required.

2. Material and methods

2.1. Material preparation and reagents

The root plant material was collected at the flowering stage from the south of the Marivan area, on the plain of Rikhalan village (35.466408, 46.185039). The botanical identification was carried out by Dr. Zeinab Toluei (Department of Biotechnology, Faculty of Chemistry, University of Kashan, Kashan, I.R. Iran) using the available literature (Mozaffarian, 1996). A voucher specimen (No. M2016.12) has been recorded at the department of cell and molecular biology, university of Kashan, Iran. Silver nitrate ($AgNO_3$), nutrient broth medium, and nutrient agar medium were purchased from Merck. The OVCAR3 human ovarian cancer cell line was supplied by the Pasteur Institute of Iran (Tehran, Iran). The Iranian research organization for science and technology (IROST) provided standard microbial strains. The clinical strains in this study were isolated from the patient's urinary tract infection (UTI) and provided by the microbiology laboratory at Shahid Beheshti Hospital, Kashan, Iran. Medical mask absorbable and non-absorbable suture silk were purchased in a local pharmacy. The experimental procedure was used to deionize water. The green synthesis method was used to synthesize AgQDs, where the aqueous fraction extract of the sample was employed to reduce $AgNO_3$ to AgQDs.

2.2. Sample preparation and extraction procedure

The plant samples were rinsed with natural water twice and dried at laboratory temperature. The dried sample was powdered and stored in a capped plastic container until extraction. The powdered sample was extracted with methanol (500 ml) using a Soxhlet extractor for 6 h. The resulting extract was filtered and evaporated (Heidolph, Rotary Evaporator, model-RE 801, Germany) at 40 °C before being dried in a vacuum oven at 35 °C. The MeOH extract (3 g dissolved in 300 ml water) was subjected to solvent–solvent partition using *n*-hexane (3 × 150 ml) and ethyl acetate (3 × 150 ml). After solvent–solvent distribution, the remained portion was used as a water fraction in the experiment.

2.3. Total phenol

The total phenolic content of the plant extracts was assessed using the colorimetric Folin-Ciocalteu assay (Velioglu et al., 1998). First, 0.1 ml of Folin Ciocalteu phenol reagent, 3 ml of distilled water, and 0.02 ml of extract (5 mg/ml) were combined. Three minutes later, 0.3 ml of sodium carbonate (2%) was added, and the mixture was measured at 760 nm using UV–Visible spectrophotometry. Similarly, the same procedure was repeated for all the standard gallic acid solutions (100–1000 μg), resulting in a standard curve with the following equation:

$$\text{Absorbance} = 0.0009 \times \text{gallic acid } (\mu g) + 0.00319$$

The results were reported in milligrams of gallic acid equivalent (GAE) per gram of extract.

2.4. Total flavonoid content (TFC)

Total flavonoid concentration was measured using a modified aluminum colorimetric procedure with quercetin as a standard (Sulastri et al., 2018). Ethanol was the solvent used to dilute the standard (10 mg) to 2, 4, 6, 8, and 10 μg/ml. Test tubes were filled with 1 ml of each concentration. In a subsequent stage, 1 ml of extract (1 mg/ml), 0.2 ml of potassium acetate (1 M), 3 ml of ethanol, 0.2 aluminum chloride (10%), and 5.6 ml of distilled water were added to each tube and then homogenized. All test tubes were kept at room temperature for 15 min. The absorbance was recorded at 376 nm using UV–Visible spectrophotometry. The flavonoid content of the extract was determined as milligram of quercetin equivalent (QE) per gram of extract.

2.5. Green synthesis of AgQDs

Different parameters, including pH, reaction temperature, the concentration of $AgNO_3$, and the concentration ratio of extract and $AgNO_3$ solution, were optimized to affect the synthesis rate of AgQDs. As a result, we conducted 32 trials to examine these factors (Table S01).

Effect of silver nitrate concentration: $AgNO_3$ solution was applied as a substrate for the reaction and silver precursor. Various concentrations of $AgNO_3$ (1, 2, 3, and 4 mM) were used to determine its effect on nanoparticle synthesis.

The concentration proportion of the plant extract and the silver nitrate solution: The concentration proportion of the extract and $AgNO_3$ solution is mutable for the optimum production of AgQDs. In this research, the reaction was performed using varied proportions of the extract and $AgNO_3$ solution (1:20, 1:50, 1:100, and 1:200).

Effect of temperature: The synthesis of AgQDs was performed at 30, 40, 50, and 60 °C. The water bath is used to maintain the reaction temperature.

Effect of pH: The optimization of pH was accomplished by adding the reaction mixture to various pH values (pH: 5, 7, 9, and 11). The pH was sustained with 0.1 N NaOH and 0.1 N HCl.

The AgQDs were synthesized by the following process:

A water fraction of the extract in a ratio of 1:50 was added to the aqueous solution of $AgNO_3$ (3 mM/l) at pH 7 and kept in the water bath (60 °C) for 12 h. The colour of solution turned dark brown, then centrifuged three times (Eppendorf, Centrifuge, model-5810R, Germany) at 9,000 rpm for 30 min (25 °C). It was then rinsed with distilled water and ethanol before being placed in the vacuum oven for 24 h.

2.6. Characterization

The UV–Vis analysis (Shimadzu, UV Spectrophotometer, model-UV1800, Japan) was accomplished to determine the absorption maxima by scanning the sample from 360 to 700 nm. X-ray diffraction (Philips/Panalytical, XRD, model X'Pert Pro, Netherlands) with a Cu Kα-radiation (λ = 1.5 4 Å) in the 2θ range from 10 to 80° was used to investigate the crystal structure of AgQDs. Fourier transform infrared spectroscopy (Nicolet Magna IR-550 FTIR) of the dry powder was recorded in 4000–400 cm^{-1} using a KBr pellet technique. Dynamic Light Scattering (DLS)-Horiba nanoparticle analyzer SZ-100 with a 532 nm laser was employed to measure particle size distribution. After sonicating the AgQDs for one hour in ethanol, the morphology and elemental fingerprinting of the resulting silver quantum dots were studied using electron microscopes (SEM: MIRA3 Tescan; EDXA: Oxford Link ISIS-300; TEM: Tecnai-12 FEI). The photoluminescence (PL) spectra were investigated by a Japan Hitachi 850 Spectrophotometer. The Nikon Eclipse Ti-s fluorescent microscope was used to record the fluorescence microscopy images, which used green and blue light as excitation sources.

2.7. Antibacterial and antifungal assays

In this study, the standard microorganisms purchased from IROST, including *Salmonella paratyphi-A serotype* (ATCC 5702), *Shigella dysenteriae* (PTCC 1188), *Staphylococcus epidermidis* (ATCC 12228), *Klebsiella pneumonia* (ATCC 10031), *Pseudomonas aeruginosa* (ATCC 27853), *Bacillus subtilis* (ATCC 6633), *Escherichia coli* (ATCC 10536), *Staphylococcus aureus* (ATCC 29737), *Proteus vulgaris* (PTCC 1182) of bacteria, *Candida albicans* (ATCC 10231) of yeast, *Aspergillus niger* (ATCC 16404) and *Aspergillus brasiliensis* (PTCC 5011) of fungi, and 60 clinical strains were isolated from the patient's UTI. Sabouraud dextrose agar (SDA) was used to culture the fungus overnight at 30 °C, while the bacterial strains were cultured overnight at 37 °C in nutrient agar (NA). According to the Clinical and Laboratory Standards Institute-CLSI (2016), the antimicrobial activities of the AgQDs were assessed using the well diffusion method. The bacterial strains were introduced into a nutrient broth medium and incubated at 37 °C for two to four hours until they attained the turbidity of the 0.5 McFarland standard. Then 100 μl of bacterial suspension was cultured on a Muller-Hinton agar plate. Then AgQDs were mixed in deionized water (30 mg/ml), and a standard drug (ampicillin 125 μg/ml) was placed as a positive control. The inoculated plates were incubated at the appropriate temperatures for 24 h. The zone of inhibition (ZI) was evaluated using a Vernier calliper to determine the antibacterial properties of the synthesized silver quantum dots.

2.8. Time-killassay

S. epidermidis and *C. albicans* were employed for the growth kinetic test because of their inhibition activities with AgQDs. At first, 1 ml each of microbial suspensions modified to 0.5 McFarland ($\approx 1 \times 10^8$ CFU/ml) was added to Trypticase soy broth (TSB) medium, including AgQDs at the minimum bactericidal concentration (MBC) level. Also, as a control, the medium containing these microbial suspensions (without AgQDs) was prepared and incubated on a rotary shaker (130 rpm) at 37 °C. The cultures were dispersed onto tryptone soya agar (TSA) agar plates at 0, 30, 90, 210, 270, 375, 435, 565, and 1260 min. The colonies were counted after incubating the plates at 37 °C for 24 h. Time-kill assay was performed three times for each strain, and the number of colony-forming units (CFU) per milliliter was measured. The growth curves with and without AgQDs were drawn according to CFU per milliliter.

2.9. DPPH radical scavenging activity

The antioxidant potential of AgQDs was evaluated using DPPH free radical scavenging (Ebrahimabadi et al., 2010). Concentrations ranging from AgQDs (0.5, 5, 50, 100, 250, 500, 800, and 1000 μg/ml) were prepared, and butylated hydroxytoluene (BHT) was applied as well as a standard for the investigation. Then, 3 ml of methanol solution of DPPH (0.1 mMol/l) was mixed with each concentration using a vortex. The reaction mixture was incubated in the dark for 30 min (room temperature), recording the activity at 517 nm. The activity was determined and reported as a percentage of inhibition based on the following equation:

$$\text{Inhibition (\%)} = \text{A control–A sample /A control} \times 100$$

A sample is the absorbance of the test sample (extract or AgQDs), and A control is the absorbance of the control reaction (which includes all reagents except the test compound). The half-maximal inhibitory concentration IC_{50} value was computed.

2.10. Cytotoxicity studies

2.10.1. MTT [3-(4,5-dimethylthiazol-2-yl)-2,5-diphenyltetrazolium bromide]

MTT assay was applied to probe the cytotoxic effects of AgQDs on the viability of OVCAR3 cells. This examination is defined by the existence of violet-colored formazan crystals from converting light yellow MTT by mitochondrial enzymes-catalyzed. Cells were seeded (5×10^5/ml) in 96 well plates and incubated overnight at 37 °C and 5% CO_2. The following day, varying concentrations of AgQDs (0–32 μg/ml) were added. 20 μl of MTT (5 mg/ml) was added to each well after 24, 48, and 72 h treatments, and then the plates were incubated at 37 °C for 4.5 h. At the end of the experiment, the medium was thrown away and replaced by 150 μl of dimethyl sulfoxide, and the plate was incubated for 20 min. An ELISA reader (Benchmark Bio-Rad) was used to determine the color absorption at a wavelength of 570 nm. The percentage of viable cells was determined using the following equation:

$$\text{viable cells \%} = (\text{OD treat/OD control}) \times 100$$

OD control and OD treatment were the optical densities of control and exposed cells, respectively. Also, the AgQDs inhibitory effect was evaluated on normal human fibroblast cells to confirm no significant side effects. GraphPad Prism software was employed to calculate the 50% lethal concentration (IC_{50}) values of AgQDs on OVCAR3 cells at various intervals.

2.10.2. Trypan blue viability assay

This dye was applied to define the number of living OVCAR3 cells after treatment with AgQDs. Initially, 10^6 OVCAR3 cells were cultured in 24-well plates and incubated for 24 h. Then, cells were exposed to AgQDs, and the cells treated with cell culture medium were considered as control. After 24 h, the cells were washed twice with PBS, and 1 ml of Trypan Blue (0.4%, Sigma-Aldrich) was added to each well and incubated for 3 min at room temperature. The unstained as viable and stained as dead cells were counted separately. Then, the percentage of cell viability was studied.

2.10.3. Brine shrimp

The brine shrimp lethality assay was performed using the Meyer et al. method with minor adaptations (Meyer et al., 1982). One of the important bioassays for determining bioactive compounds is brine shrimp lethality (Zhao et al., 1992). The brine shrimp *Artemia salina* was selected in this experiment as a feasible monitor for the screening. The artificial seawater (3.8% NaCl solution) is used to hatch the eggs of the brine shrimp for 48 h to become mature shrimp, also called nauplii. Seawater (3.8% NaCl in water) was added to the samples (dissolved in DMSO, 3.2%) to obtain concentrations of 10 μg/ml, 100 μg/ml, 300 μg/ml, 500 μg/ml, 700 μg/ml, 1000 μg/ml. The positive and negative controls were vincristine sulphate (VS) and DMSO. The lethality percentage was computed by comparing the mean number of dead larvae in the test and control tubes. Afterward, matured shrimps were used in each experimental and control vial. The number of surviving nauplii in each vial was determined after 24 h. The lethal concentration of silver quantum dots causes a 50% mortality of brine shrimp (LC_{50}) was calculated based on counts and dose–response data. The mortality percentage was computed as follows:

$$\text{Mortality percentage} = [(\text{m} - \text{M})/\text{S}] \times 100$$

In this equation, M is the average number of dead larvae in the blank control, S is the average number of live larvae in the blank control, and m is the average number of dead larvae in the sample.

2.10.4. Ames assay (-S9)

Salmonella typhimurium strains TA100 and TA98 used for the assay (-S9) were obtained from BioReliance Corporation (Rockville, MD, USA) (Maron and Ames, 1983). The genotype, crystal violet sensitivity, UV light sensitivity, ampicillin antibiotic resistance or sensitivity, and lack of growing power in plates without biotin and histidine assays were evaluated to confirm the strains. Strains (TA100, TA98) were incubated for 5 h at 37 °C, shaking at 75 rpm. The synthesized AgQDs were dispersed in sterilized water by vortexing and sonicating for 5 min. For performing the Ames test, AgQDs (200–400 μg/plate), 100 μl Biotin (12.4 μg/plate), 100 μl histidine (9.6 μg/plate), 0.5 ml of phosphate buffer, and 100 μl bacterial culture were added to 2 ml of molten top agar and shed on glucose minimum agar. They were gently rotated, similar to the infinity symbol. The plates were inverted and incubated at 37 °C for 65–70 h. These assays were conducted three times for statistical analysis. The positive controls for strain TA98 and strain TA100 were 4-Nitro-o-phenylenediamine (5 μg/plate) and sodium azide (5 μg/plate), respectively. Dimethyl sulfoxide (DMSO) is used as a negative control. Mutation induction relative to the negative control as induction factors (IF) were calculated for each AgQDs concentration. The antimutagenic effects of the AgQDs were evaluated according to percentage inhibitory.

$$\text{\% inhibition} = [1 - (\text{T}/\text{M})] \times 100$$

M is the number of revertants per plate (positive control)
T is the number of revertants per plate (presence of mutagen)
The antimutagenic effect is considered strong (more than 40%), moderate (25–40%), and weak (less than 25%).

2.11. AgQDs coating on the chosen materials

This research selected eight items (absorbable and non-absorbable suture silk, medical mask fabric, yarn, filter paper, cotton, toothpick, and cotton fabric) to develop the antimicrobial activity. The selected materials were soaked in the silver solution and then subjected to a UV lamp (k = 365 nm, t = 10 min) to induce the synthesized AgQDs on their surface (Pollini et al., 2008).

2.12. Cellular uptake and bioimaging

The AgQDs solution was mixed with cell culture media and OVCAR3 cells and then incubated for 2 h to see if they could be used as fluorescent markers for cellular imaging. Before the cells were fixed on the slide for examination under a fluorescent microscope, the excess AgQDs were eliminated by washing them three times in phosphate-buffered saline (PBS). Afterward, live-cell imaging was performed under bright fields, green (480 nm), and blue (360 nm) excitations.

2.13. Statistical analysis

The measurements were conducted in triplicate, and the results were presented as mean values ± SD (standard deviations). Statistical software SPSS for windows (Version 21) was employed for analysis.

3. Results and discussion

3.1. Bioactivity of extract:

The analytical findings for the DPPH radical-scavenging capacity, phenolic, and flavonoid content of the extract are shown in Table 1. The extract illustrated significant antioxidative activity in the DPPH test (IC_{50} = 56.23 ± 2.85 μg/ml), which was more than the synthetic antioxidant butylated hydroxyl toluene (BHT: IC_{50} = 18.15 ± 1.33 μg/ml). The total phenolic and flavonoid content was 97.12 ± 3.15 and 45.86 ± 1.56 mg/g, respectively. The results demonstrate that the extract has total phenolic and flavonoid content. It is demonstrated that the antioxidant activity of *T. polium* extract is attributed to flavonoids and phenolic compounds (Bahramikia and Yazdanparast, 2012). Several phenolic components from *T. polium* extract have been identified, such as isorhoifolin, cirsilineol, apigenin, cirsiliol, and poliumoside (Venditti, 2017).

3.2. Characterization of silver quantum dots

The colorless $AgNO_3$ solution slowly turned a brown or deep red after adding the extract. UV–Visible data showed that some designed experiments could synthesize AgQDs and give intense peaks ranging from 410 nm to 460 nm (SPR) (Kashyap et al., 2019). The absorption spectra revealed an intense peak, indicating increased AgQDs production. The intense peak at 419 nm was obtained in pH 7, 1 ml of the extract in 50 ml of $AgNO_3$ solution (3 mM) at 60 °C. Based on the findings, this condition was identified as the most effective for synthesizing green AgQDs Therefore, we chose these conditions for further analysis (Fig S1-S4). Fig. 1 summarizes the effects of contact time on nanoparticle formation under the same conditions.

The Infrared spectrum of the eco-friendly synthesized silver quantum dots was analyzed to identify the functional group using FTIR spectroscopy. In Fig. 2, the peak at 3439 cm^{-1}, 1384 cm^{-1}, and 824 cm^{-1} display the formation of quantum dots. The strong stretching vibrations of the O–H functional group were identified in the IR peak spectra at 3439. The sharp peak observed at 1324 cm^{-1} corresponds to nitro N-O bending, and the peak of 824 cm^{-1} indicates the C–H, C–C phenyl ring substitutes (Mahadevan et al., 2017).

The XRD pattern (Fig. 3) of silver quantum dots revealed the noticeable peaks at 2θ = 38.11°, 44.09°, 64.52°, 77.37°, representing the (1 1 1), (2 0 0), (2 2 0), and (3 1 1) Bragg's reflections of the face-centered cubic structure of silver, respectively. The average crystalline size (D) of the AgQDs was determined using the Debye-Scherrer formula, which is given as $D = 0.9\lambda/\beta\cos\theta$. Where θ is the Bragg angle (in degrees), β is the angular line width at half maximum intensity (in radians), and λ is the X-ray wavelength (in nm). For maximum intensity at $2\theta \approx 38.11$, β = 0.00824 rad, λ = 1.54Å, and $\theta \approx 19.05$, Scherrer's equation was used to estimate the average size of the Ag nanoparticles, which is estimated to be around 17.90 nm (Nazari and Jookar Kashi, 2021).

The small and uniformly spherical nanoparticles are confirmed by the SEM images (Fig. 4a) of the sample obtained from the colloidal Ag solutions. The SEM images show that larger particles of AgQDs are organized due to the assemblage of nanoparticles, which solvent evaporation might induce during sample preparation. This could have played a key role in the particle size change. An SEM equipped with an EDAX

Table 1 Total phenolic, flavonoid contents and antioxidant activities of extract of *T. Polium*.

Total phenolic mg GAE/g extract	Total flavonoids mg QE/g extract	IC_{50} of DPPH radical (μg/ml)	
		Extract	**BHT**
97.12 ± *3.15*	45.86 ± 1.56	56.23 ± 2.85	18.15 ± 1.33

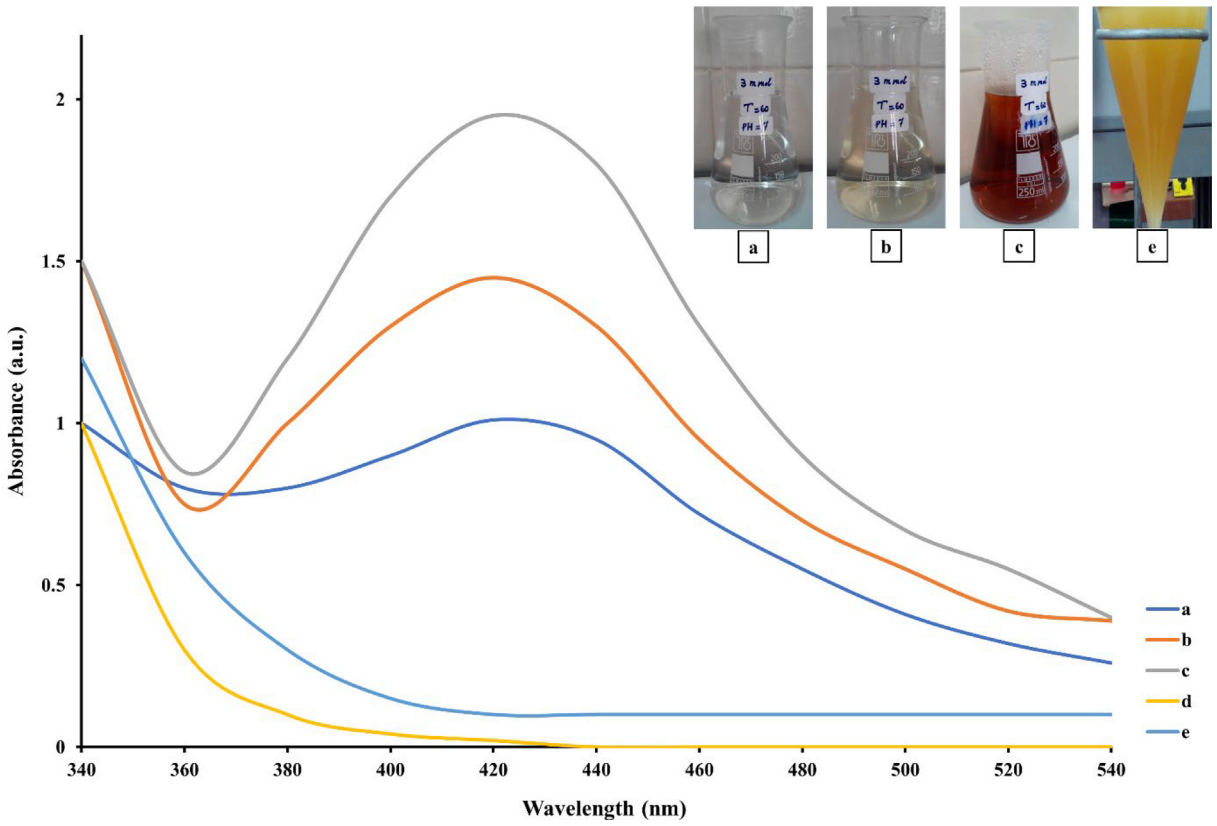

Fig. 1 UV–vis absorption spectra of AgQDs: *T. polium* extract + $AgNO_3$ solution at different time intervals (a = 1 min, b = 30 min, c = 180 min), $AgNO_3$ solution (Ag^+) (d), *T. polium* extract (e).

detector was used to evaluate the elemental composition of the sample. The energy dispersive X-ray analysis (EDAX) in Fig. 4b showed a strong signal in 3 keV related to silver and indicated the successful formation of AgQDs. Following the literature, metallic AgQDs show strong surface plasmon resonance (SPR) at 3 keV (Ismail et al., 2018). As shown in Fig. 4 (b), the appearance and percentages of C (0.77%), N (2.37%), O (7.48%), and Ag (89.39%) confirmed that the formations of metallic AgQDs are free of impurities. A transmission electron microscope (TEM) was used to investigate the size and shape of the organized nanoparticles. Fig. 4c shows that silver quantum dots exhibited considerable uniformity with a narrow distribution. The TEM image of silver quantum dots indicates spherical, with an average size of about 12 nm under their size distribution histograms (Fig. 4d). A DLS instrument was employed to analyze the size distribution of the AgQDs. The results demonstrated that the particle size for silver quantum dots synthesized using a 3 mM sample was around 4 nm. The DLS method is commonly used to determine particle size distribution in colloidal solutions. The TEM result and the size distribution of AgQDs obtained by DLS are comparable. In 2020, Hashemi et al. synthesized silver nanoparticles using the water extract of *T. polium,* which was collected from Kerman, Iran. Compared to the obtained AgQDs in our study, the average size of the nanoparticles was greater (range 70–100 nm) (Hashemi et al., 2020). Pugazhenthiran et al. synthesized AgQDs using aqueous extracts of sweet lime peels in another research study. They dissolved 5 ml of extract in 20 ml of $AgNO_3$ solution (2 mM/l) at 80 °C. In contrast to our report, the synthesized nanoparticles had lower absorption at 415 nm. Moreover, in the current research, AgQDs were synthesized at 60 °C in an affordable and eco-friendly neutral environment (Pugazhenthiran et al., 2021).

3.3. PL

Photoluminescence has been observed in metal nanoparticles such as Au and Ag (Khalil et al., 2012; Vinay et al., 2019). Fig. 5a displays the room temperature PL emission spectrum of AgQDs in the wide range of 320–450 nm. The excitation peaks were 210 to 310 nm (ten by ten). The strong band emission from 340 to 430 nm was repeatably recorded. This range belongs to the violet emission region. The emission band was reported at 487 nm upon excitation at 432 nm for synthesized AgQDs using Tamarind fruit extract (Jayaprakash et al., 2017). Fig. 5 shows the fluorescence microscopic images of OVCAR3 cells treated with AgQDs for 4 h under a bright field (Fig. 5. b1) and different excitation wavelengths of 480 nm (Fig. 5. b2) and 360 nm (Fig. 5. b3). Microscopic images of AgQDs-labeled OVCAR3 cells as a fluorescent probe demonstrated prominent green and blue emissions. The penetration of the AgQDs into the cells with their fluorescent properties in the cellular environment was demonstrated by green and blue-colored luminescence in the nuclei. In contrast, the luminescence in the cytoplasm was extremely feeble. The AgQDs obtained solution was strongly fluorescent under UV-A (365 nm), whereas the $AgNO_3$ solution and empty vial as control had no fluorescent light (Fig. 5c).

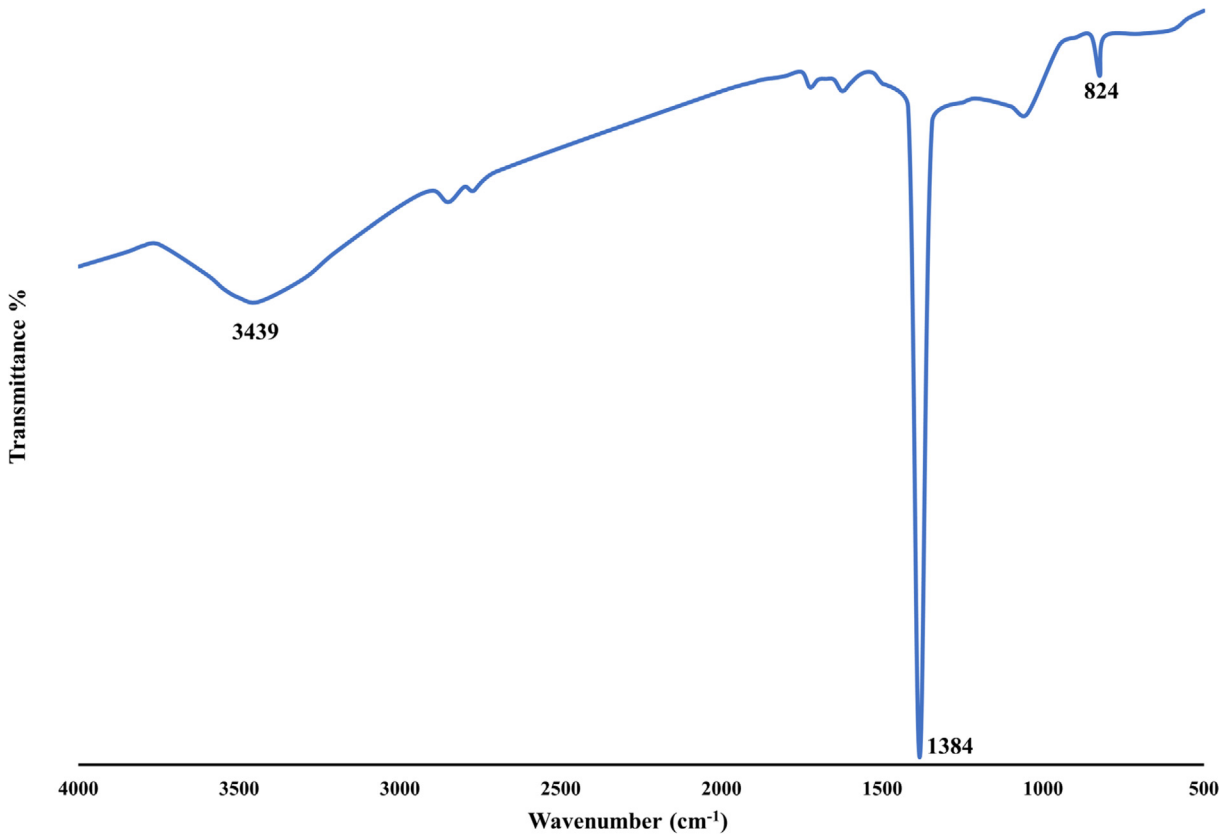

Fig. 2 FT-IR spectra of biosynthesized AgQDs.

4. Bioactivities

4.1. Antimicrobial activity

The minimum inhibitory concentration (MIC) values were measured for samples and antibiotics with notable inhibiting effects on the growth of bacteria. The biosynthesized AgQDs were prepared with dilutions ranging from 31.25 to 500 µg/ml. The MIC results of the samples and antibiotics for standard and clinical strains are shown in tables 2 and 3, respectively. These results showed that *S. epidermidis* and *C. albicans* were more sensitive than gram-negative bacteria. *K. pneumonia*, *S. dysenteriae*, and *S. paratyphi-Aserotype* have shown more resistance to AgQDs. The antimicrobial activity of AgQDs against *E. coli* was reported by Ibrahim. Their results displayed that the zone of inhibition was 17 mm, which is better than the synthesized AgQDs in our investigation (Ibrahim, 2015).

The results showed that clinical strains were more resistant than standard strains. Further, AgQDs indicated high antimicrobial activity compared with $AgNO_3$. The inhibition zone diameter of AgQDs and $AgNO_3$ was (10–35 mm) and (8–14 mm), respectively. AgQDs have a higher surface-to-volume ratio than silver nitrate. At the nanoscale, the optical, electrical, and catalytic properties change. Due to their unique properties, these materials manufacture products for targeted drug delivery, diagnosis, imaging, and antimicrobial agents. Therefore, the characteristics of silver nanoparticles have made them suitable for use in medical and health products and the treatment or prevention of infections (Bruna et al., 2021). Moreover, AgQDs have deeper contact with microorganisms because of their vast surface area, and AgQDs are a source of Ag +. For these reasons, AgQDs might cause high antimicrobial activity.

Mahadevan et al. synthesized silver nanoparticles from *Atalantia monophylla* (L) Correa leaf extract, which illustrated that the nanoparticles had antimicrobial activity against *S. aureus* (37 mm), *B. cereus* (36 mm), and *C. albicans* (34 mm) (Mahadevan et al., 2017). Furthermore, in research by Bapat et al., the antimicrobial activity of green silver nanoparticles was evaluated using the disc diffusion method. Based on the findings, the nanoparticles displayed feeble antibacterial activity against the chosen bacterial strains (Bapat et al., 2022). In another research, the antibacterial activity of biosynthesized AgNPs displayed an inhibition zone of 14.93 ± 0.57 mm against *S. aureus* (Das et al., 2019). Moreover, green synthesized AgNPs using *Cicer arietinum* showed moderate antibacterial activity against pathogenic Gram-negative (*E. coli* (14 ± 0.5 mm), *S. aureus* (13 ± 1 mm)) and Gram-positive (*P. aeruginosa* (13 ± 0.5 mm), *B. cereus* (10 ± 0.5 mm)) (Mouriya et al., 2023). Kordzangeneh and Jookar Kashi evaluated the antibacterial effect of Ag/AgCl composite against bacterial strain. Their results showed that the composite had antibacterial and antibiofilm activities (Kordzangeneh and Jookar Kashi, 2022). The results of other study revealed that *P. aeruginosa* (14.18 ± 0.02 mm) was the most sensitive to AgNPs, rather than *S. aureus* (12.18 ± 0.02 mm) and *E. coli*

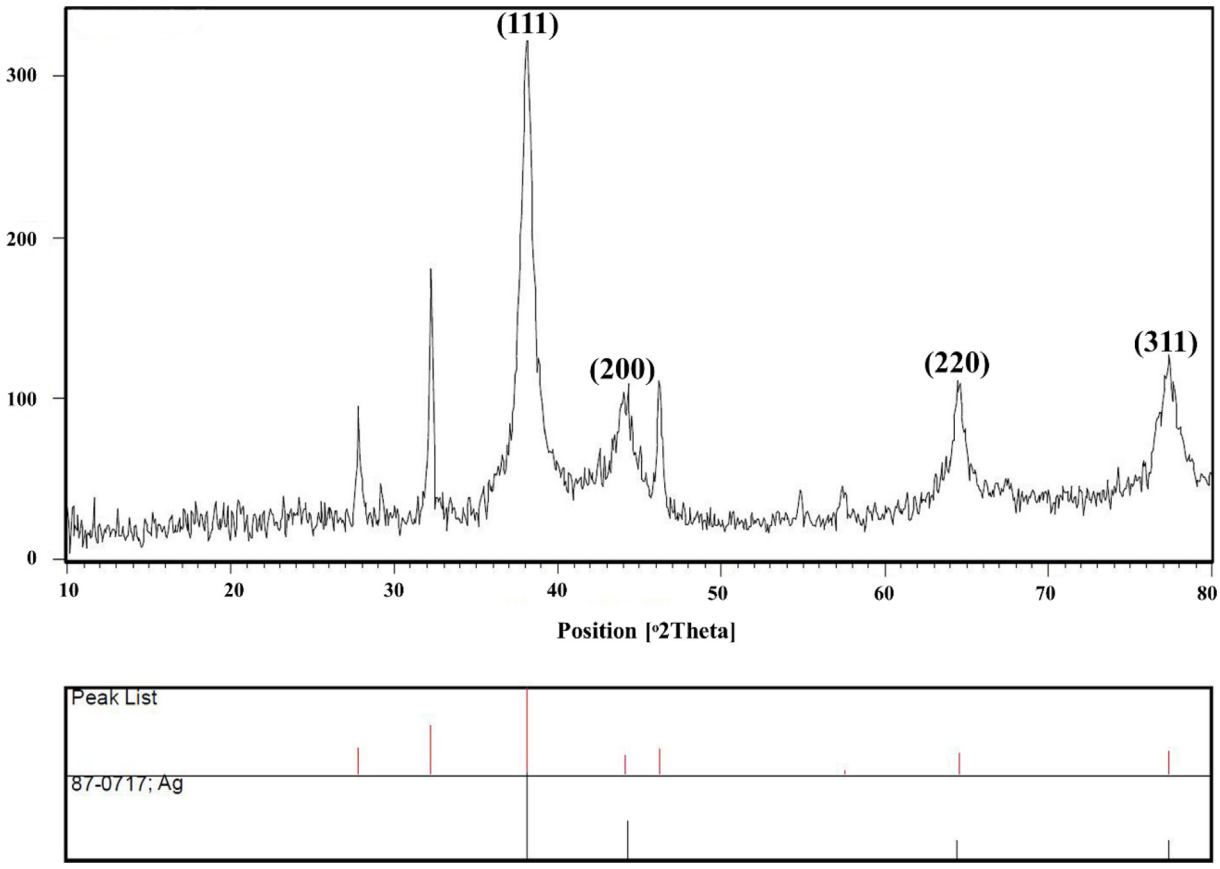

Fig. 3 X-ray diffraction patterns of AgQDs.

(12.16 ± 0.03 mm) (Singh et al., 2023). The results showed that silver nanoparticles synthesized using different fruits have antimicrobial effects on *S.aureus*, *B.cereus*, *E.coli*, and *C. krusei* (Wasilewska et al., 2023). Rakhshan et al. reported that green synthesized nanoparticles have antimicrobial activity against *B.subtilis* (Rakhshan et al., 2022). Antimicrobial effects are probably due to the attachment of AgQDs to bacterial cell walls, membranes, and proteins and the change in DNA conformations, leading to the death of the bacterial cell. Moreover, we proposed that AgQDs produce free radicals, which are also considered an important factor in the mechanism by which the cell dies. Scheme 1. demonstrates our suggested mechanisms for the antibacterial activity of AgQDs.

The colony counter assay has been used to estimate the density of microorganisms in liquid culture by counting individual colonies on an agar plate. In our study, a colony counting assay was performed to determine the number of viable bacteria cells in a plate after being treated with the AgQDs. The minimum bactericidal concentration (MBC) of nanoparticulate for *S. epidermidis* and *C. albicans* was the same (62.5 µg/ml). Using time–kill assays, populations of bacteria organisms tested in the presence of 62.5 µg/ml AgQDs were increased from 0 to 400 min (Fig. 6). In the presence of AgQDs (62.5 µg/ml), *S. epidermidis* populations were decreased to zero in 565 min. Populations of *S. epidermidis* and *C. albicans* were reduced to % 27.27 and % 21.9, respectively, from 375 to 435 min.

4.2. Brine shrimp

The number of brine shrimp larvae that survived after 24 h was counted, and the LC_{50} value was calculated. The brine shrimp lethality assay (LC_{50}) for AgQDs and the positive control (vincristine sulfate) was 6.21 µg/ml and 0.751 µg/ml, respectively. The green synthesis AgQDs of *T. Polium* L. showed considerable brine shrimp larvicidal activity. This research is the first report on brine shrimp lethality activity of fluorescent silver quantum dots using *T. Polium* L. Our results illustrated that the brine shrimp cytotoxicity assay could be an easy bioassay to screen nanoparticles. Using the brine shrimp assay to indicate cytotoxicity and antitumor activity is conceivable. The positive correlation of the brine shrimp cytotoxicity experiment suggests that the nanoparticles could be a source of cytotoxicity, which may support their usage as an anticancer agent or carrier. As a result, the cytotoxic effect of nanoparticles can be related to their size and shape. However, AgQDs can cure a wide range of infections and prevent cancer. In research by Kummara et al., the anticancer activity of green and chemically synthesized AgQDs was evaluated using the brine shrimp method. They demonstrated that silver nanoparticles had high cytotoxicity and anticancer activity (Kummara et al., 2016). Furthermore, in research by Alam, cytotoxicity assessment of green synthesis silver nanoparticles using strawberry fruit pomace extract showed high cytotoxic activity with an LC_{50} value of 200 µg/ml (Alam, 2022). In another research, Nazari

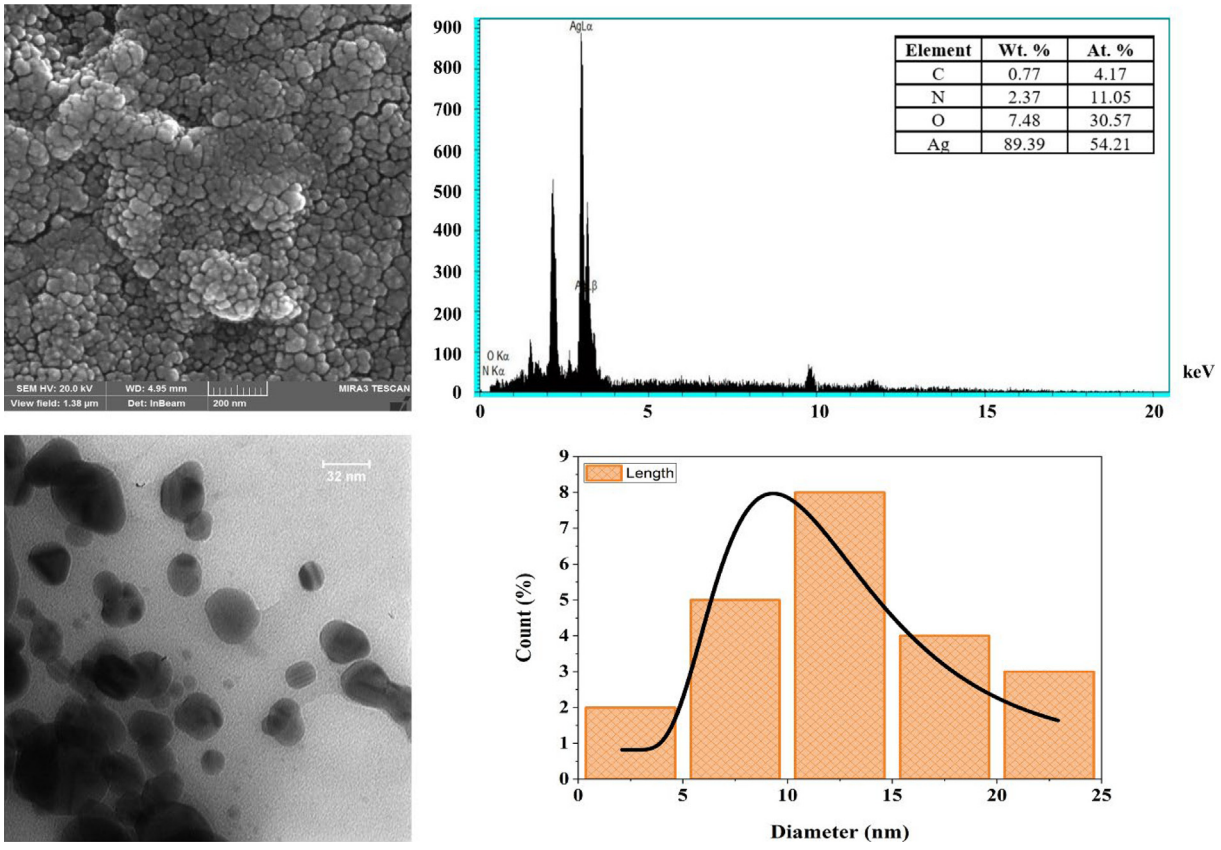

Fig. 4 SEM (a), EDX spectrum (b), TEM (c) images, and the size distribution histogram (d) of AgQDs.

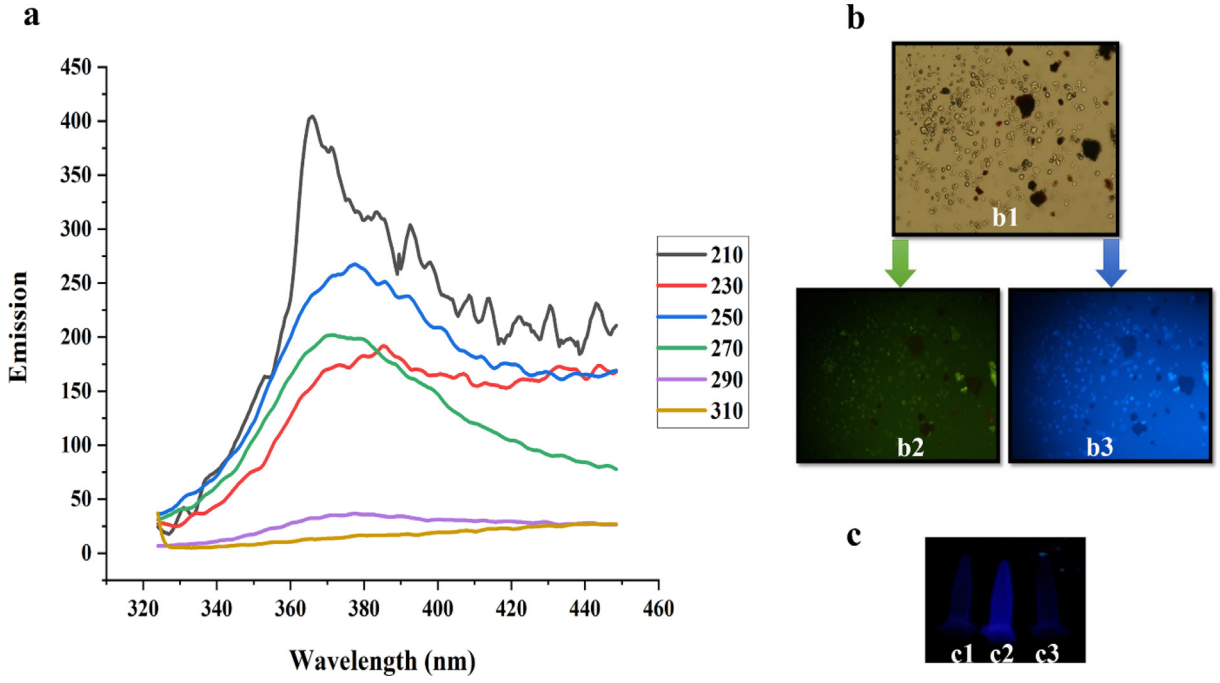

Fig. 5 (**a**) PL emission spectra of the AgQDs obtained by excitation wavelengths from 210 to 310 nm. (**b**) b1 (A bright-field microphotograph of the OVCAR3 cells), b2 (A fluorescence microphotograph of OVCAR3 cells labeled with the AgQDs (λex: 480 nm)), b3 A fluorescence microphotograph of OVCAR3 cells labeled with the AgQDs (λex: 360 nm)). (**c**) Samples under UV-A (365 nm) light: c1 ($AgNO_3$ solution), c2 (AgQDs solution), c3 (empty vial).

Table 2 AgQDs against standard microbial strains.

Standard strain	Antibiotics						Sample			
	Rifampin		Gentamicin		Nystatin		AgQDs		$AgNO_3$	
Microbial strain	DD[a]	MIC[b]	DD	MIC	DD	MIC	DD	MIC	DD	MIC
	Gram-positive bacteria									
B. subtilis	12.3 ± 0.57	125	19.6 ± 1.52	500	NA[c]	NA	15.6 ± 0.57	125	–	–
S. epidermidis	39 + 1	500	34.3 ± 1.15	500	NA	NA	34.3 ± 0.57	31.25	13.3 ± 0.57	31.25
S. aureus	9.3 ± 0.57	500	20 ± 1.73	500	NA	NA	17.3 ± 1.15	62.5	8 ± 0.0	31.25
	Gram-negative bacteria									
E. coli	–	–	21.6 ± 1.52	500	NA	NA	9.6 ± 0.57	500	8 ± 1.0	31.25
K. pneumonia	10.3 ± 0.57	500	18.6 ± 1.52	500	NA	NA	–	–	10.6 ± 0.57	31.25
S. dysenteriae	8 ± 0.0	500	17 ± 1.0	500	NA	NA	–	–	10.3 ± 1.15	31.25
P. vulgaris	9.3 ± 1.15	500	21.3 ± 1.52	500	NA	NA	12.6 ± 1.52	500	–	–
S. paratyphi-Aserotype	–	–	20 ± 1.73	500	NA	NA	–	–	9.33 ± 1.15	31.25
P. aeruginosa	7 ± 0.0	500	20.6 ± 1.15	250	NA	NA	11.3 ± 0.57	500	8.6 ± 0.57	125
	Fungi									
C. albicans	NA	NA	NA	NA	NA	NA	31 ± 1.0	31.25	11.6 ± 0.57	62.5
A. niger	NA	NA	NA	NA	33	125	–	–	–	–
A. brasilienis	NA	NA	NA	NA	NA	NA	–	–	–	–

A dash(-) indicate no antimicrobial activity.
[a] Inhibition zone in diameter (mm) around the impregnated discs.
[b] Minimal inhibition concentrations (as μg/ml).
[c] Plant samples were inactive against mould in disc diffusion test so that the MIC agar dilution test for nystatin was not carried out. NA (not applicable).

Table 3 AgQDs against clinical bacterial strains.

Clinical strain		AgQDs	
Microbial strain	No. samples	DD[a]	MIC[b]
Staphylococcus epidermidis	6	32.8 ± 0.75	31.25
Candida albicans	8	30.1 ± 0.64	31.25
Proteus vulgaris	7	12.1 ± 0.69	500
Enterococcus faecalis	2	–	–
Acinetobacter baumannii	7	–	–
Staphylococcus saprophyticus	7	13 ± 0.81	125
Staphylococcus aureus	4	16 ± 0.82	62.5
Salmonella paratyphi	2	–	–
Escherichia coli	5	9.8 ± 0.84	500
Klebsiella pneumonia	7	–	–
Pseudomonas syringae	5	–	–

A dash (-) indicate no antimicrobial activity.
[a] Inhibition zone in diameter (mm) around the impregnated discs.
[b] Minimal inhibition concentrations (as μg/ml).

et al. employed *Marinospirillum alkaliphilum* to synthesize AgNPs and examined its anticancer properties using the brine shrimp assay. According to their studies, the nanoparticles were highly toxic (LC_{50} = 1 μg/ml) (Nazari and Jookar Kashi, 2021). We believe that our results are accurate.

4.3. Ames

Cancer has risen as a global health concern that involves over 100 different kinds of abnormal cell division with the property of metastasis (Barabadi et al., 2020; Vahidi et al., 2020). Nanomaterials could be used to develop next-generation anticancer agents. Hence, newly produced nanoparticles should be thoroughly investigated. The Ames test is one of the methods used to determine if nanoparticles have anticancer effects. Therefore, bacterial mutagenicity and antimutagenicity of AgQDs were assessed. The experiment was organized only in the absence of S9 since AgQDs were metal, and it was improbable that S9 would metabolize them. Strain TA98 and strain TA100 detected mutagens that caused various frameshift and base-pair substitutions. The AgQDs were nontoxic for *S. typhimurium* strains at the performed concentration. The mutagenicity and antimutagenic effects of the AgQDs are summarized in Table 4. A substance with an induction factor of two or greater is considered a mutant. The number of returned colonies depends on the concentration and has a dose-dependent effect. The sample is not mutagenic if the induction factor is less than 1.5, and between 1.5 and 2 represents poor mutagenicity (Dashtizadeh et al., 2021). In addition to this, the anti-mutagenicity effect of the sample with three levels of weak, medium, and strong was assumed to be below 20%, between 40% and 25%, and more than 40%, respectively (Espanha et al., 2014). It was discovered that strain TA98 produces the best response from the tested nanoparticles. For the highest AgQDs concentration (400 μg), the largest number of reverted colonies was discovered, which displayed a maximum induction factor (IFmax) of 1.18 and 1.13 for strains TA98 and TA100, respectively. Although, none of the tested nanoparticle concentrations led to any mutation induction. Moreover, statistical data evaluation showed they were significantly higher than the control induction. The results of colony counting in the Ames test using silver quantum dots showed a significant anti-mutagenic effect on colony growth. In addition, prevention percent was used to determine the prevented reverted mutations of AgQDs in the anti-mutagenicity test. The AgQDs

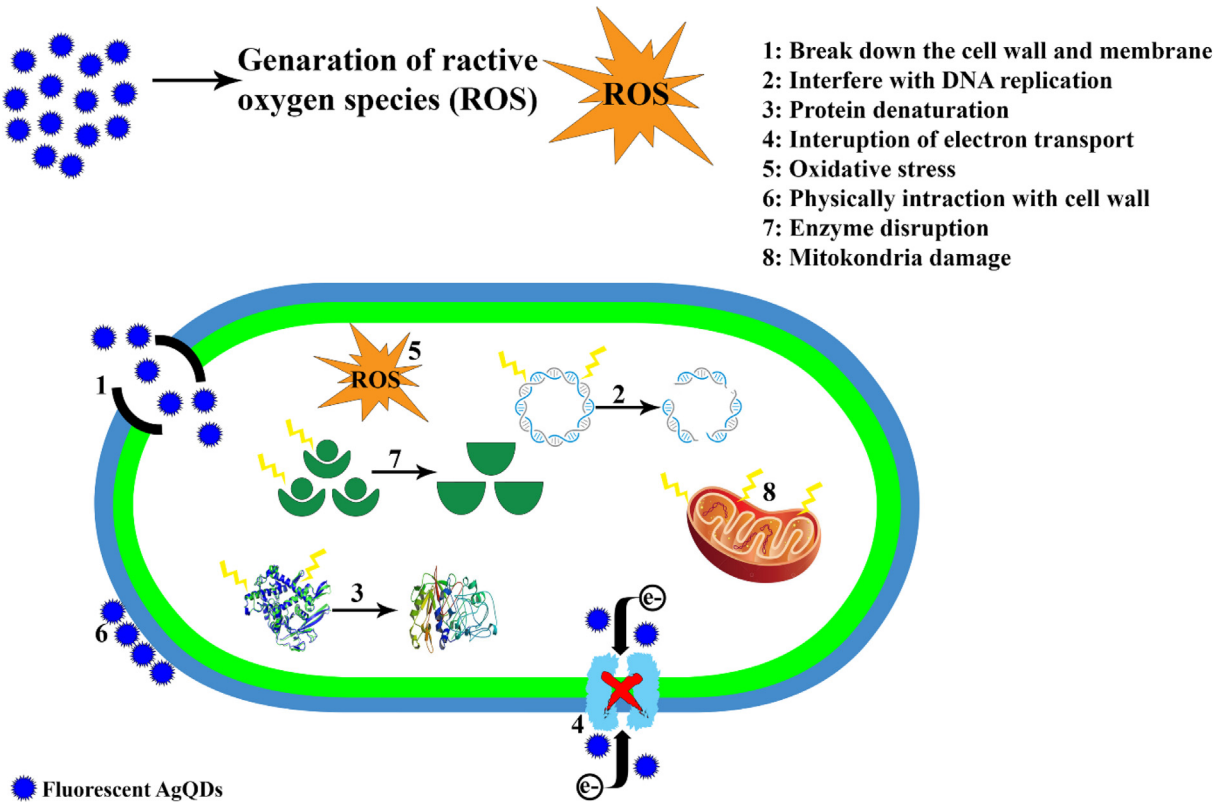

Scheme 1 The proposed mechanisms for the antibacterial activity of AgQDs.

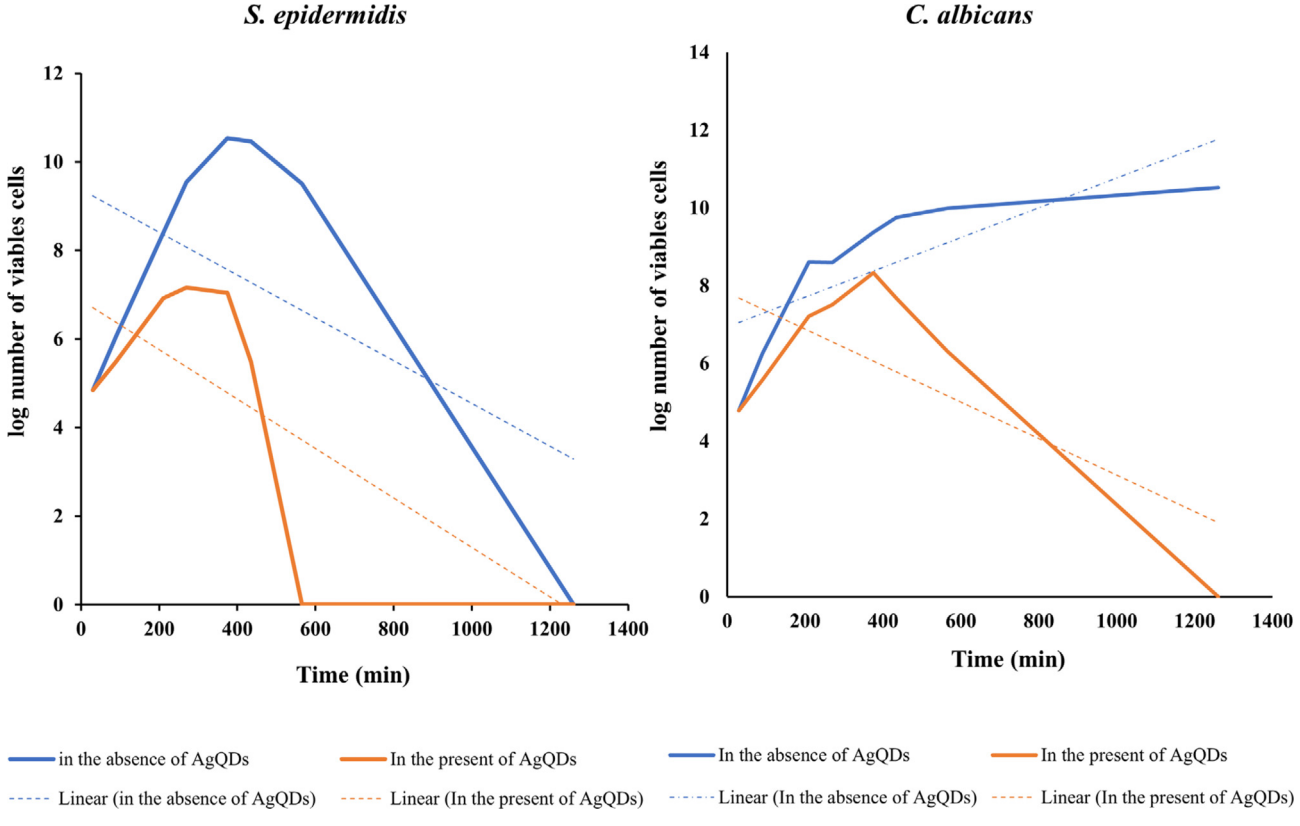

Fig. 6 Growth curves of *S. epidermidis* and *C. albicans* in the absence and presence of AgQDs at concentration of MBC (62.5 μg/ml).

Table 4 Results of (a) mutagenicity and (b) antimutagenicity test of AgQDs on strains TA98 and TA100.

a	C(μg/plate)	-S9 IF[c]		b	C(μg/plate)	-S9 Prevention percent			
		TA_{98}	TA_{100}			TA_{98}		TA_{100}	
	400	1.18	1.13			NC[d]	PC[e]	NC	PC
	300	1.16	1.05		200	88.04	84.56	80.94	78.48
	200	1.08	1.01		300	88.76	85.59	82.17	79.78
	Negative control	1	1		400	89.47	86.43	82.81	80.62
					Positive control	6.25	5.21		

c: Induction factor, d: Negative control, e: Positive control.

(400 μg) represented the highest prevention percentage (89.47%). The findings prove that the AgQDs have antimutagenicity activity, confirming the brine shrimp test. Nikouharf Fakher et al. determined the mutagenic effects of synthesized Ag/AgCl nanoparticles on strains TA100 and TA98. They have demonstrated that the nanoparticles did not show a mutagenic effect, and their percent inhibition of mutagenicity was more than 97% (Fakher and Kashi, 2021). In another study, Khan et al. evaluated the mutagenic properties of synthesized AgNPs using an aqueous extract of *Pinus wallichiana* stem against strains TA98 and TA100. They concluded that the nanoparticles were nontoxic and nonmutagenic (Khan et al., 2020).

4.4. MTT

AgQDs as therapeutic agents is limited, although it has shown antimicrobial activities and biological applications (Mohanty et al., 2012). Our research determined the sensitivity of OVCAR3 cells to AgQDs through an MTT assay. As displayed in Fig. 7, AgQDs considerably decreased the proliferation of OVCAR3 cells in a time- and dose-dependent manner. The IC_{50} of AgQDs was 5.9, 2.3, and 0.8 μg/ml in OVCAR3 cells after 24, 48, and 72 h, respectively. It was proven that AgQDs concentrations ranging from 0 to 0.25 μg had no prominent cytotoxic effect on the OVCAR3 cells. The AgQDs indicated no considerable cytotoxic effects at 0.5 μg/ml concentration after 24 h. On the other hand, approximately 23% of the cells were viability dosed at 8 μg/ml after 72 h. Also, trypan blue viability assay results were consistent with the MTT assay. The cell viability was equal after 48 and 72 h at 16 μg/ml. The biosynthesized silver nanoparticles by (Hamelian et al., 2018) showed that the viability of Hela cells was even up to 200 μg/ml after 48 h. Previous research on green synthesized AgNPs from *Piper longum* extract demonstrated that viability in vitro cytotoxic properties against Hep-2 cells was observed at 49% in 31.25 μg/ml concentration (Justin Packia Jacob et al., 2012). Furthermore, increased

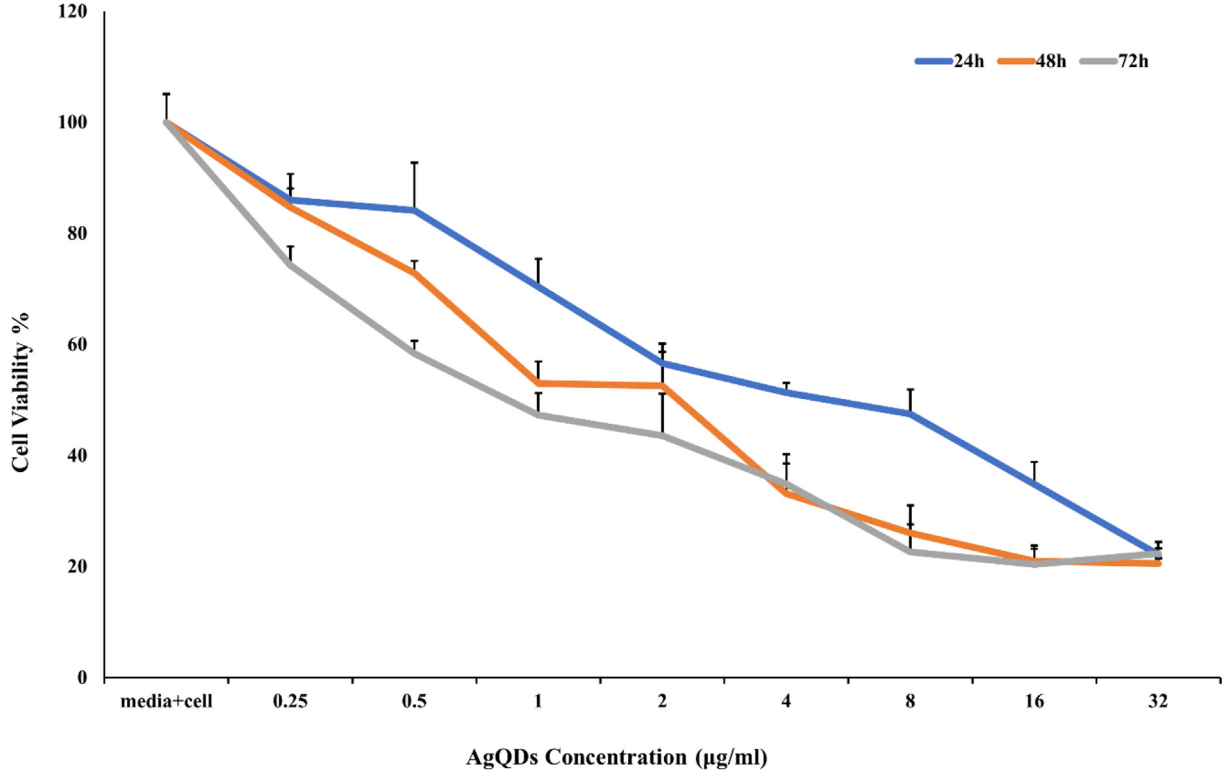

Fig. 7 Cytotoxic of AgQDs synthesized against OVCAR3 cell line after 24, 48, and 72 h.

cytotoxicity of AgNPs on the MCF-7 cell line was displayed with increasing concentration (Selvi et al., 2016). In another study, silver nanoparticles indicated a selective cytotoxic effect against cancer cells (IC_{50} = 82.016 μg/ml) and a non-toxic effect in normal fibroblast cells (Mouriya et al., 2023). Moreover, the study of the cytotoxicity of AgNPs against MCF 7, Hela, and OP9 cell lines demonstrated synergistic effects on cytotoxicity (Ghosal et al., 2020).

4.5. The effect of AgQDs on normal cells

The results of the inhibitory effect of the AgQDs on normal human fibroblast cells showed that the AgQDs had an insignificant effect on normal human fibroblast cells at concentrations near IC_{50} of AgQDs on cancer cells after 24, 48, and 72 h.

The AgQDs killed normal cells in 16%, 20%, and 24% after 24, 48, and 72 h, respectively. These findings confirmed that these doses of AgQDs have no considerable side effects (Fig. 8).

4.6. DPPH

In this method, the IC_{50} of AgQDs was 4.8 μg/ml proving that AgQDs have higher antioxidant activity than BHT (IC_{50} = 18.15 μg/ml). Two oxidation states (i.e., Ag^{+} and Ag^{2+}) can exist for silver, so silver-based nanoparticles may be able to remove free radicals by donating or accepting electrons based on the reaction environments. The experiment results found that the antioxidant activity of AgQDs is relevant to their concentrations. The findings also revealed the substantial increase in antioxidant activity of green synthesized AgQDs compared to *T. polium* extract. According to the results, we proposed that the AgQDs are responsible for most of the antioxidant activity. Kanipandian et al. synthesized silver nanoparticles using *Cleistanthus collinus* extract. They found that the DPPH radical scavenging capacity was enhanced with plant extract, similar to our research (Kanipandian et al., 2014). Yousaf et al. studied the synthesis of silver nanoparticles using methanol, ethanol, and aqueous extracts of *A. millefolium*. They found that silver nanoparticles synthesized from methanol extract showed significant antioxidant properties (IC_{50} = 7.03 ± 0.31 μg/ml) compared to the ascorbic acid standard (IC_{50} = 4.29 ± 1.74 μg/ml) (Yousaf et al., 2020). Researchers have shown that the strong scavenging ability of silver nanoparticles might be dependent on donating electrons or hydrogen ions to neutralize the unstable DPPH free radicals in the reaction environment (Bardania et al., 2020).

4.7. Coating material by AgQDs

Antimicrobial activity (agar diffusion tests) was carried out on silver-treated and untreated (as control) toothpicks, cotton, medical mask fabric, cotton fabric, non-absorbable suture silk, absorbable suture silk, yarn, and filter paper against *C.albicans* and *S.epidermidis* strains. Fig. 9 shows the results of the agar diffusion test. Hence, a well-marked inhibition zone was revealed around the silver-treated items, pointing out the significant efficacy of the materials against gram-positive (*S.epidermidis*) bacteria and yeast (*C.albicans*). However, untreated samples showed no antibacterial efficacy. The results displayed that the antibacterial silver-coated sutures developed in this investigation could be an affordable alternative to general sutures. Moreover, other silver-treated materials, such as spinning and cosmetics, can be suggested for industrial applica-

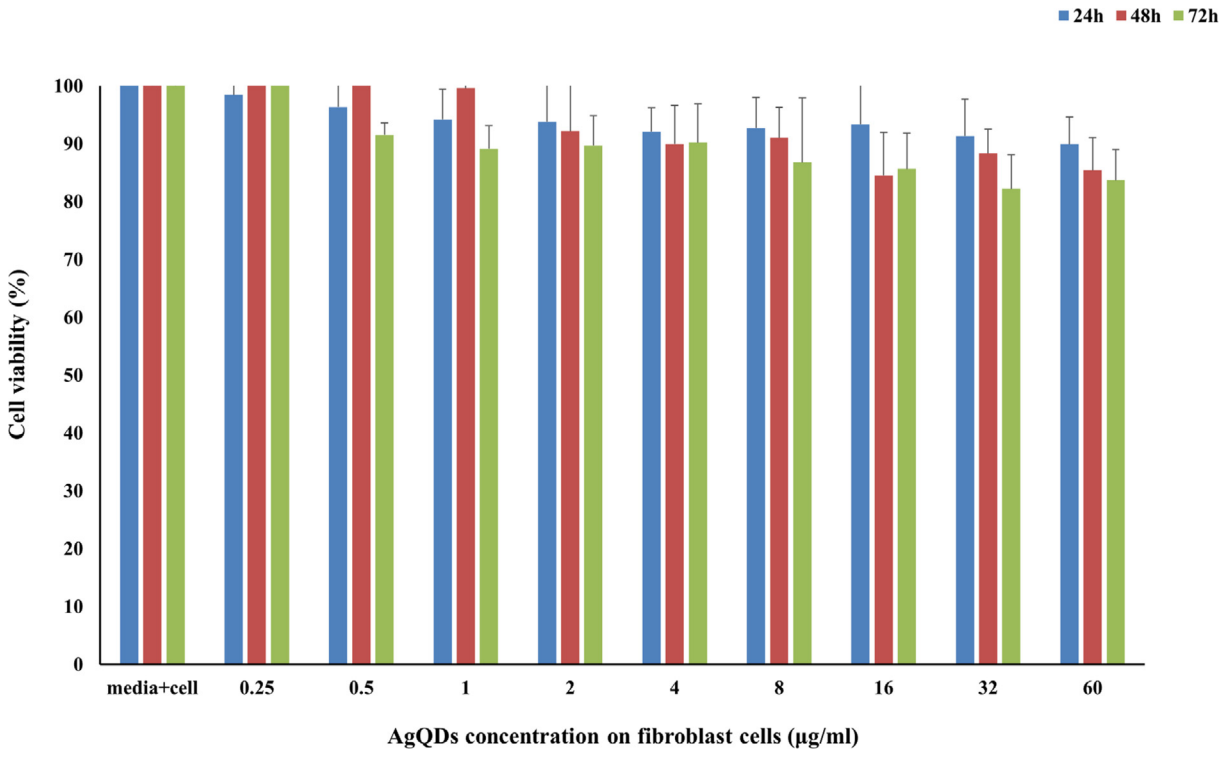

Fig. 8 Cytotoxic of AgQDs synthesized against normal human fibroblast cells after 24, 48, and 72 h.

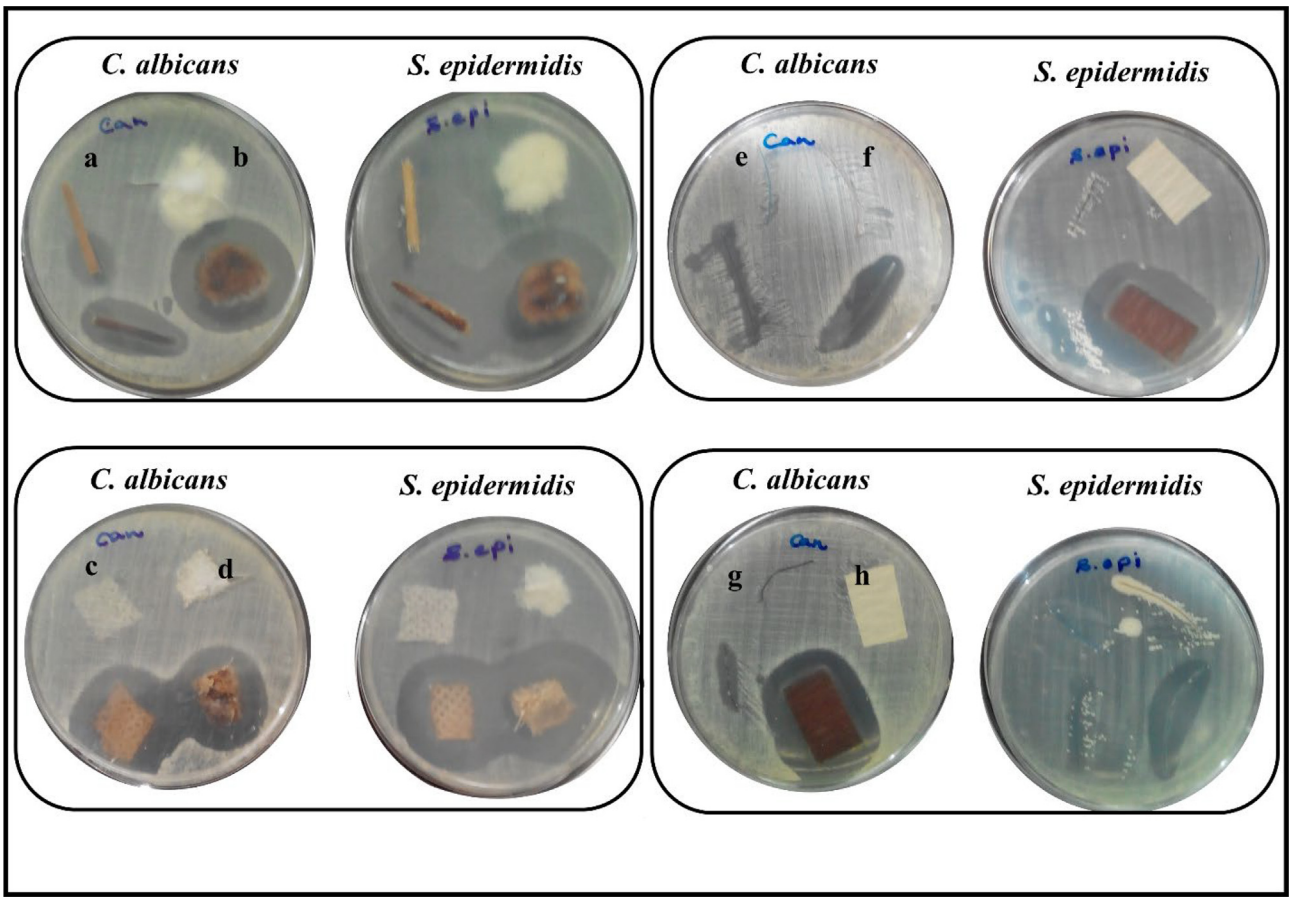

Fig. 9 Antimicrobial test for untreated and silver treated on a: toothpick b: cotton c: medical mask fabric d: cotton fabric e: non-absorbable suture silk f: absorbable suture silk g: yarn h: filter paper against *C. albicans* and *S. epidermidis*.

tions. Simone et al. reported that silver-treated suture silk could represent clinical advantages in preventing surgical infections (De Simone et al., 2014). In another research, Sharma et al. produced silver nano-coated fabric and evaluated antimicrobial activity against *E. coli* and *S. aureus*. They discovered that fabric treated with nanoparticles effectively against *S.aureus* (Sharma et al., 2018).

5. Conclusion

The most apparent discovery of this study is that a plant extract can synthesize AgQDs in a green and environmentally acceptable manner, providing a cost-effective, simple, and efficient way. *T. Polium* collected from the south of the Marivan area, Iran, had antioxidant activities due to its substantial phenols and flavonoid content. The solvent–solvent partition of *T. Polium* extract was employed to produce green AgQDs. The chemical constituents of the extract play a vital role in the production of AgQDs. The AgQDs spherical shape showed high antioxidant, cytotoxic, anti-mutagenicity, and antimicrobial properties. Moreover, AgQDs are photoluminescent with 320 to 450 nm emission bands and are not mutagenic. Due to the high antimicrobial property, the green synthesized AgQDs were applied for the antimicrobial investigation to support the hypothesis of nano-coated materials that would possess noteworthy antimicrobial activity. Biosynthesized AgQDs exhibit diverse biological activities. Therefore, the AgQDs are a suitable candidate for many biomedical and industrial applications, including biosensors, uniform materials, surfaces and coatings, and textiles.

Acknowledgement

We are grateful to thank for providing the chemicals used in this study by the Natural Essential Oil Research Institute, University of Kashan (Grant No. 96/26077). Thanks are also extended to Dr. Zeinab Toluei (Department of Biotechnology, Faculty of Chemistry, University of Kashan, Kashan, I.R. Iran), who helped the author identify the plant.

Appendix A. Supplementary data

Supplementary data to this article can be found online at https://doi.org/10.1016/j.arabjc.2023.104811.

References

Agressott, E.V.H., de Moura, T.A., Marinho, N.L., de L. Vasconcelos, T., Cunha, F.A., Fechine, P.B.A., de Souza Filho, A.G., Paschoal, A.R., 2020. Tip-Enhanced Raman spectroscopy investigations of core-shell Ag-proteins nanoparticles synthesized by Rhodotorula mucilaginosa and Rhodotorula glutinis fungi. Vibrational Spectroscopy 110, 103104. 10.1016/j.vibspec.2020.103104.

Alam, M., 2022. Analyses of biosynthesized silver nanoparticles produced from strawberry fruit pomace extracts in terms of biocompatibility, cytotoxicity, antioxidant ability, photodegrada-

tion, and in-silico studies. Journal of King Saud University - Science 34,. https://doi.org/10.1016/j.jksus.2022.102327 102327.

Ali, M., Khan, T., Fatima, K., Ali, Q., ul, A., Ovais, M., Khalil, A.T., Ullah, I., Raza, A., Shinwari, Z.K., Idrees, M., 2018. Selected hepatoprotective herbal medicines: Evidence from ethnomedicinal applications, animal models, and possible mechanism of actions. Phytother. Res. 32, 199–215. https://doi.org/10.1002/ptr.5957.

Aromal, S.A., Vidhu, V.K., Philip, D., 2012. Green synthesis of well-dispersed gold nanoparticles using Macrotyloma uniflorum. Spectrochim. Acta A Mol. Biomol. Spectrosc. 85, 99–104. https://doi.org/10.1016/j.saa.2011.09.035.

Bahramikia, S., Yazdanparast, R., 2012. Phytochemistry and Medicinal Properties of *Teucrium polium* L. (Lamiaceae): MEDICINAL PROPERTIES OF *T. POLIUM*. Phytother. Res. 26, 1581–1593. https://doi.org/10.1002/ptr.4617.

Bapat, M.S., Singh, H., Shukla, S.K., Singh, P.P., Vo, D.-V.-N., Yadav, A., Goyal, A., Sharma, A., Kumar, D., 2022. Evaluating green silver nanoparticles as prospective biopesticides: An environmental standpoint. Chemosphere 286,. https://doi.org/10.1016/j.chemosphere.2021.131761 131761.

Barabadi, H., Vahidi, H., Damavandi Kamali, K., Rashedi, M., Hosseini, O., Saravanan, M., 2020. Emerging Theranostic Gold Nanomaterials to Combat Colorectal Cancer: A Systematic Review. J Clust Sci 31, 651–658. https://doi.org/10.1007/s10876-019-01681-x.

Bardania, H., Mahmoudi, R., Bagheri, H., Salehpour, Z., Fouani, M. H., Darabian, B., Khoramrooz, S.S., Mousavizadeh, A., Kowsari, M., Moosavifard, S.E., Christiansen, G., Javeshghani, D., Alipour, M., Akrami, M., 2020. Facile preparation of a novel biogenic silver-loaded Nanofilm with intrinsic anti-bacterial and oxidant scavenging activities for wound healing. Sci Rep 10, 6129. https://doi.org/10.1038/s41598-020-63032-5.

Bruna, T., Maldonado-Bravo, F., Jara, P., Caro, N., 2021. Silver Nanoparticles and Their Antibacterial Applications. IJMS 22, 7202. https://doi.org/10.3390/ijms22137202.

Das, P., Ghosal, K., Jana, N.K., Mukherjee, A., Basak, P., 2019. Green synthesis and characterization of silver nanoparticles using belladonna mother tincture and its efficacy as a potential antibacterial and anti-inflammatory agent. Mater. Chem. Phys. 228, 310–317. https://doi.org/10.1016/j.matchemphys.2019.02.064.

Dashtizadeh, Z., Jookar Kashi, F., Ashrafi, M., 2021. Phytosynthesis of copper nanoparticles using Prunus mahaleb L. and its biological activity. Materials Today. Communications 27,. https://doi.org/10.1016/j.mtcomm.2021.102456 102456.

De Simone, S., Gallo, A.L., Paladini, F., Sannino, A., Pollini, M., 2014. Development of silver nano-coatings on silk sutures as a novel approach against surgical infections. J Mater Sci: Mater Med 25, 2205–2214. https://doi.org/10.1007/s10856-014-5262-9.

Ebrahimabadi, A.H., Ebrahimabadi, E.H., Djafari-Bidgoli, Z., Kashi, F.J., Mazoochi, A., Batooli, H., 2010. Composition and antioxidant and antimicrobial activity of the essential oil and extracts of Stachys inflata Benth from Iran. Food Chem. 119, 452–458. https://doi.org/10.1016/j.foodchem.2009.06.037.

Edison, T.J.I., Sethuraman, M.G., 2012. Instant green synthesis of silver nanoparticles using Terminalia chebula fruit extract and evaluation of their catalytic activity on reduction of methylene blue. Process Biochem. 47, 1351–1357. https://doi.org/10.1016/j.procbio.2012.04.025.

Elbahnasawy, M.A., Shehabeldine, A.M., Khattab, A.M., Amin, B. H., Hashem, A.H., 2021. Green biosynthesis of silver nanoparticles using novel endophytic Rothia endophytica: Characterization and anticandidal activity. J. Drug Delivery Sci. Technol. 62,. https://doi.org/10.1016/j.jddst.2021.102401 102401.

Espanha, L.G., Resende, F.A., de Sousa Lima Neto, J., Boldrin, P.K., Nogueira, C.H., de Camargo, M.S., De Grandis, R.A., dos Santos, L.C., Vilegas, W., Varanda, E.A., 2014. Mutagenicity and antimutagenicity of six Brazilian Byrsonima species assessed by the Ames test. BMC Complement Altern Med 14, 182. https://doi.org/10.1186/1472-6882-14-182.

Fakher, S.N., Kashi, F.J., 2021. Microbial Synthesized Ag/AgCl Nanoparticles Using Staphylococcus pasteuri sp. nov., ZAR1: Antimutagenicity. Antimicrobial Agent. J Inorg Organomet Polym 31, 1688–1703. https://doi.org/10.1007/s10904-021-01879-5.

Ghosal, K., Ghosh, S., Ghosh, D., Sarkar, K., 2020. Natural polysaccharide derived carbon dot based in situ facile green synthesis of silver nanoparticles: Synergistic effect on breast cancer. Int. J. Biol. Macromol. 162, 1605–1615. https://doi.org/10.1016/j.ijbiomac.2020.07.315.

Hamelian, M., Zangeneh, M.M., Amisama, A., Varmira, K., Veisi, H., 2018. Green synthesis of silver nanoparticles using *Thymus kotschyanus* extract and evaluation of their antioxidant, antibacterial and cytotoxic effects: Biosynthesis of silver nanoparticles using Thymus kotschyanus extract. Appl Organometal Chem 32, e4458.

Hashemi, S.F., Tasharrofi, N., Saber, M.M., 2020. Green synthesis of silver nanoparticles using Teucrium polium leaf extract and assessment of their antitumor effects against MNK45 human gastric cancer cell line. J. Mol. Struct. 1208,. https://doi.org/10.1016/j.molstruc.2020.127889 127889.

He, F.J., Li, Z.H., Gao, F., Yang, Z., 2013. Extracellular Biosynthesis of Ag Nanoparticles by Commercial Baker's Yeast. AMR 785–786, 370–373. https://doi.org/10.4028/www.scientific.net/AMR.785-786.370.

Ibrahim, H.M.M., 2015. Green synthesis and characterization of silver nanoparticles using banana peel extract and their antimicrobial activity against representative microorganisms. J. Radiat. Res. Appl. Sci. 8, 265–275. https://doi.org/10.1016/j.jrras.2015.01.007.

Ismail, M., Khan, M.I., Khan, S.B., Akhtar, K., Khan, M.A., Asiri, A. M., 2018. Catalytic reduction of picric acid, nitrophenols and organic azo dyes via green synthesized plant supported Ag nanoparticles. J. Mol. Liq. 268, 87–101. https://doi.org/10.1016/j.molliq.2018.07.030.

Jadoun, S., Arif, R., Jangid, N.K., Meena, R.K., 2021. Green synthesis of nanoparticles using plant extracts: a review. Environ Chem Lett 19, 355–374. https://doi.org/10.1007/s10311-020-01074-x.

Jayaprakash, N., Vijaya, J.J., Kaviyarasu, K., Kombaiah, K., Kennedy, L.J., Ramalingam, R.J., Munusamy, M.A., Al-Lohedan, H.A., 2017. Green synthesis of Ag nanoparticles using Tamarind fruit extract for the antibacterial studies. J. Photochem. Photobiol. B Biol. 169, 178–185. https://doi.org/10.1016/j.jphotobiol.2017.03.013.

Justin Packia Jacob, S., Finub, J.S., Narayanan, A., 2012. Synthesis of silver nanoparticles using Piper longum leaf extracts and its cytotoxic activity against Hep-2 cell line. Colloids Surf. B Biointerfaces 91, 212–214. https://doi.org/10.1016/j.colsurfb.2011.11.001.

Kalimuthu, K., Cha, B.S., Kim, S., Park, K.S., 2020. Eco-friendly synthesis and biomedical applications of gold nanoparticles: A review. Microchem. J. 152,. https://doi.org/10.1016/j.microc.2019.104296 104296.

Kanipandian, N., Kannan, S., Ramesh, R., Subramanian, P., Thirumurugan, R., 2014. Characterization, antioxidant and cytotoxicity evaluation of green synthesized silver nanoparticles using Cleistanthus collinus extract as surface modifier. Mater. Res. Bull. 49, 494–502. https://doi.org/10.1016/j.materresbull.2013.09.016.

Kashyap, M., Samadhiya, K., Ghosh, A., Anand, V., Shirage, P.M., Bala, K., 2019. Screening of microalgae for biosynthesis and optimization of Ag/AgCl nano hybrids having antibacterial effect. RSC Adv. 9, 25583–25591. https://doi.org/10.1039/C9RA04451E.

Khalil, M.M.H., Ismail, E.H., El-Magdoub, F., 2012. Biosynthesis of Au nanoparticles using olive leaf extract. Arab. J. Chem. 5, 431–437. https://doi.org/10.1016/j.arabjc.2010.11.011.

Khan, N., Khan, I., Nadhman, A., Azam, S., Ullah, I., Ahmad, F., Khan, H.A., 2020. *Pinus wallichiana* -synthesized silver nanoparticles as biomedical agents: in-vitro and in-vivo approach. Green Chem. Lett. Rev. 13, 69–82. https://doi.org/10.1080/17518253.2020.1733105.

Kordzangeneh, H., Jookar Kashi, F., 2022. A new Bacillus Paralicheniformis sp. Tmas-01 as bioreactor for synthesis of Ag/AgCl composite–different effects of biological and Rodamin B dye decolorization, anticancer, genotoxic activity. Arch Microbiol 204, 706. https://doi.org/10.1007/s00203-022-03317-7.

Kummara, S., Patil, M.B., Uriah, T., 2016. Synthesis, characterization, biocompatible and anticancer activity of green and chemically synthesized silver nanoparticles – A comparative study. Biomed. Pharmacother. 84, 10–21. https://doi.org/10.1016/j.biopha.2016.09.003.

Mahadevan, S., Vijayakumar, S., Arulmozhi, P., 2017. Green synthesis of silver nano particles from Atalantia monophylla (L) Correa leaf extract, their antimicrobial activity and sensing capability of H 2 O 2. Microb. Pathog. 113, 445–450. https://doi.org/10.1016/j.micpath.2017.11.029.

Maron, D.M., Ames, B.N., 1983. Revised methods for the Salmonella mutagenicity test. Mutation Research/Environmental Mutagenesis and Related Subjects 113, 173–215. https://doi.org/10.1016/0165-1161(83)90010-9.

Meyer, B., Ferrigni, N., Putnam, J., Jacobsen, L., Nichols, D., McLaughlin, J., 1982. Brine Shrimp: A Convenient General Bioassay for Active Plant Constituents. Planta Med 45, 31–34. https://doi.org/10.1055/s-2007-971236.

Mohan Kumar, K., Mandal, B.K., Sinha, M., Krishnakumar, V., 2012. Terminalia chebula mediated green and rapid synthesis of gold nanoparticles. Spectrochim. Acta A Mol. Biomol. Spectrosc. 86, 490–494. https://doi.org/10.1016/j.saa.2011.11.001.

Mohanty, S., Mishra, S., Jena, P., Jacob, B., Sarkar, B., Sonawane, A., 2012. An investigation on the antibacterial, cytotoxic, and antibiofilm efficacy of starch-stabilized silver nanoparticles. Nanomedicine: Nanotechnology. Biology and Medicine 8, 916–924. https://doi.org/10.1016/j.nano.2011.11.007.

Mouriya, G.K., Mohammed, M., Azmi, A.A., Khairul, W.M., Karunakaran, T., Amirul, A.-A.-A., Ramakrishna, S., Santhanam, R., Vigneswari, S., 2023. Green synthesis of Cicer arietinum waste derived silver nanoparticle for antimicrobial and cytotoxicity properties. Biocatal. Agric. Biotechnol. 47,. https://doi.org/10.1016/j.bcab.2022.102573 102573.

Mozaffarian, V., 1996. Encyclopedia of Iranian plants. Farhang Moaser Publication, Tehran, Iran, p. 671.

Nazari, N., Jookar Kashi, F., 2021. A novel microbial synthesis of silver nanoparticles: Its bioactivity, Ag/Ca-Alg beads as an effective catalyst for decolorization Disperse Blue 183 from textile industry effluent. Sep. Purif. Technol. 259,. https://doi.org/10.1016/j.seppur.2020.118117 118117.

Pollini, M., Sannino, A., Maffezzoli, A., Licciulli, A., 2008. Antibacterial surface treatments based on silver clusters deposition. EP1986499A2.

Pugazhenthiran, N., Murugesan, S., Muneeswaran, T., Suresh, S., Kandasamy, M., Valdés, H., Selvaraj, M., Dennyson Savariraj, A., Mangalaraja, R.V., 2021. Biocidal activity of citrus limetta peel extract mediated green synthesized silver quantum dots against MCF-7 cancer cells and pathogenic bacteria. J. Environ. Chem. Eng. 9,. https://doi.org/10.1016/j.jece.2021.105089 105089.

Rakhshan, N., Mansournia, M., Kashi, F.J., 2022. A Novel Bacterial Route to Synthesize Cu Nanoparticles and Their Antibacterial Activity. J Clust Sci 33, 2559–2572. https://doi.org/10.1007/s10876-021-02176-4.

Selvi, B.C.G., Madhavan, J., Santhanam, A., 2016. Cytotoxic effect of silver nanoparticles synthesized from *Padina tetrastromatica* on breast cancer cell line. Adv. Nat. Sci: Nanosci. Nanotechnol. 7,. https://doi.org/10.1088/2043-6262/7/3/035015 035015.

Shameli, K., Bin Ahmad, M., Jaffar Al-Mulla, E.A., Ibrahim, N.A., Shabanzadeh, P., Rustaiyan, A., Abdollahi, Y., Bagheri, S., Abdolmohammadi, S., Usman, M.S., Zidan, M., 2012. Green Biosynthesis of Silver Nanoparticles Using Callicarpa maingayi Stem Bark Extraction. Molecules 17, 8506–8517. https://doi.org/10.3390/molecules17078506.

Sharma, P., Pant, S., Rai, S., Yadav, R.B., Sharma, S., Dave, V., 2018. Green synthesis and characterization of silver nanoparticles by *ALLIUM CEPA L.* to produce silver nano-coated fabric and their antimicrobial evaluation. Appl Organometal Chem 32, e4146.

Singh, C., Anand, S.K., Upadhyay, R., Pandey, N., Kumar, P., Singh, D., Tiwari, P., Saini, R., Tiwari, K.N., Mishra, S.K., Tilak, R., 2023. Green synthesis of silver nanoparticles by root extract of Premna integrifolia L. and evaluation of its cytotoxic and antibacterial activity. Mater. Chem. Phys. 297,. https://doi.org/10.1016/j.matchemphys.2023.127413 127413.

Sulastri, E., Zubair, M.S., Anas, N.I., Abidin, S., Hardani, R., Yulianti, R., Aliyah, A.A., 2018. Total Phenolic, Total Flavonoid, Quercetin Content and Antioxidant Activity of Standardized Extract of Moringa oleifera Leaf from Regions with Different Elevation. PJ 10, s104–s108. https://doi.org/10.5530/pj.2018.6s.20.

Vahidi, H., Barabadi, H., Saravanan, M., 2020. Emerging Selenium Nanoparticles to Combat Cancer: a Systematic Review. J Clust Sci 31, 301–309. https://doi.org/10.1007/s10876-019-01671-z.

Vanlalveni, C., Lallianrawna, S., Biswas, A., Selvaraj, M., Changmai, B., Rokhum, S.L., 2021. Green synthesis of silver nanoparticles using plant extracts and their antimicrobial activities: a review of recent literature. RSC Adv. 11, 2804–2837. https://doi.org/10.1039/D0RA09941D.

Velioglu, Y.S., Mazza, G., Gao, L., Oomah, B.D., 1998. Antioxidant Activity and Total Phenolics in Selected Fruits, Vegetables, and Grain Products. J. Agric. Food Chem. 46, 4113–4117. https://doi.org/10.1021/jf9801973.

Venditti, A., 2017. Secondary metabolites from Teucrium polium L. collected in Southern Iran. Arabian Journal of Medicinal and Aromatic Plants Vol 3, 108-123 Pages. 10.48347/IMIST.PRSM/AJMAP-V3I2.9213.

Vinay, S.P., Udayabhanu, Nagarju, G., Chandrappa, C.P., Chandrasekhar, N., 2019. Enhanced photocatalysis, photoluminescence, and anti-bacterial activities of nanosize Ag: green synthesized via Rauvolfia tetraphylla (devil pepper). SN Appl. Sci. 1, 477. https://doi.org/10.1007/s42452-019-0437-0.

Wasilewska, A., Klekotka, U., Zambrzycka, M., Zambrowski, G., Święcicka, I., Kalska-Szostko, B., 2023. Physico-chemical properties and antimicrobial activity of silver nanoparticles fabricated by green synthesis. Food Chem. 400,. https://doi.org/10.1016/j.foodchem.2022.133960 133960.

Yousaf, H., Mehmood, A., Ahmad, K.S., Raffi, M., 2020. Green synthesis of silver nanoparticles and their applications as an alternative antibacterial and antioxidant agents. Mater. Sci. Eng. C 112,. https://doi.org/10.1016/j.msec.2020.110901 110901.

Zhao, G., Hui, Y., Rupprecht, J.K., McLaughlin, J.L., Wood, K.V., 1992. Additional Bioactive Compounds and Trilobacin, a Novel Highly Cytotoxic Acetogenin, from the Bark of Asimina triloba. J. Nat. Prod. 55, 347–356. https://doi.org/10.1021/np50081a011.